
**Liquid Crystals**
Publication details, including instructions for authors and subscription information:
http://www.informaworld.com/smpp/title~content=t713926090

# Molecular dynamics simulations of a liquid crystalline molecule in the smectic A and E phases and in vacuum

Kuei-Jen Lee; Ging-Ho Hsiue; Jung-Lung Wu; Jr-Hong Chen

Online publication date: 06 August 2010

**To cite this Article** Lee, Kuei-Jen , Hsiue, Ging-Ho , Wu, Jung-Lung and Chen, Jr-Hong(1999) 'Molecular dynamics simulations of a liquid crystalline molecule in the smectic A and E phases and in vacuum', Liquid Crystals, 26: 4, 469 — 482
**To link to this Article: DOI:** 10.1080/026782999204903
**URL:** http://dx.doi.org/10.1080/026782999204903

LIQUID CRYSTALS, 1999, VOL. 26, NO. 4, 469–482

# Molecular dynamics simulations of a liquid crystalline molecule in the smectic A and E phases and in vacuum

KUEI-JEN LEE
Deh Yu College of Nursing and Management, Keelung, Taiwan 203, ROC

GING-HO HSIUE*, JUNG-LUNG WU, and JR-HONG CHEN
Department of Chemical Engineering, National Tsing Hua University, Hsinchu, Taiwan 30043, ROC

(*Received 25 November 1996; in final form 2 January 1998; accepted 15 April 1998*)

Molecular dynamics simulations are performed in this work at 393 and 323 K for a mesogenic molecule (*R*)-1-methylheptyl 4[4-(2-allyloxyethoxy)biphenyl-4′-carbonyloxy]benzoate in the simulated smectics A and E, respectively, and in a vacuum at 300 K, for a period of 1.0 ns. The trajectories obtained from molecular dynamics simulations allow us to investigate the dynamical behaviour of this mesogenic molecule in the simulated smectic phases. This dynamical behaviour of a single molecule is presented using the distributions of dihedral angles and rotational diffusion around the C-axis defined by the simulated cells. Simulation results indicate that, except for the bonds near the end of the spacer segment, the dihedral angles all exhibit a single Gaussian-like distribution in the smectic A and E phases. Fluctuations of a dihedral angle about its mean value are more restricted in the smectics A and E than in those simulated in a vacuum. The average value of the fluctuations of the dihedral angles at the bonds in the spacer is found to be about 2 fold larger than that of fluctuations in the tail of the same molecule in the smectic A and E phases. In the smectic A phase, the distribution of orientations of a molecule about its long axis in a 36 molecule cell in which the outer molecules are fixed is found to have three distinct peaks. This result shows that the orientational fluctuations of single molecules are limited by confinement due to neighbouring molecules, i.e. that the layers have short-range structural correlations. The orientational distributions show larger fluctuations at the ends of the molecules.



## 1. Introduction

Smectic liquid crystals [1], which have been revealed as a variety of layered phases [2], have found significant applications as electro-optical materials, such as in display devices, waveguide switching, optical computing, and non-linear optics [3]. Each smectic phase has unique layer structures and tilt angles, and is characterized by both the orientational and positional order. Hsiue *et al.* [4–6] extensively studied smectic liquid crystals containing oligooxyethylene spacers, various chiral moieties, and two or three aromatic rings of ester core units, many of which have high values of ferroelectricity. This work is primarily focused on the dynamics of one kind of mesogenic molecule by using molecular dynamics simulations. In our previous work, these mesogenic molecules have been investigated not only experimentally [7] but also by atom-based molecular modelling [8].

Mesogenic molecules in the smectic phases can exhibit surprising dynamical behaviour. If observations focus on the dynamical behaviour of a molecule that is located at the centre of a simulated cell in the smectic phase, such behaviour is similar to that of chain molecules confined in unusual environments. Molecular dynamics simulations have been performed in some restrictive environments, e.g. polymers confined in the channel of crystalline perhydrotriphenylene [9–13] or in the channel of crystalline urea [14–17], to study the transitions of rotational isomeric states and mobilities of these polymers. In studies of the dynamics of molecules, molecular dynamics simulations can be a highly effective tool in identifying the connection between molecular motions and experimental parameters determined by solid-state nuclear magnetic resonance (NMR). Deuterium NMR is an appropriate technique to observe experimentally motions of molecules in the solid state. The rotation of a methyl group or the flip of a phenyl group can be easily deduced from solid-state deuterium NMR line shapes [18]. Previous investigations have applied deuterium NMR relaxation experiments to characterize restricted molecular motions in liquid crystalline systems

*Author for correspondence.

*Journal of Liquid Crystals* ISSN 0267-8292 print/ISSN 1366-5855 online 
http://www.tandf.co.uk/JNLS/lct.htm
http://www.taylorandfrancis.com/JNLS/lct.htm

[19–23]. The data obtained from deuterium spin-lattice relaxation measurements are governed by the spectral densities of motion $J_0(0)$, $J_1(\omega_0)$, and $J_2(2\omega_0)$, which are derived for application to uniaxially ordered liquid crystals [19–23]. These spectral densities have also been applied to probing the motions of molecules confined in urea clathrates [15, 24].

Selwyn *et al.* [20] studied deuterium relaxation data for thermotropic smectic liquid crystals. They used rotational diffusion on a cone as a model to account for the molecular dynamics of the smectic phases. In addition, rotational diffusion on a cone was developed as a model for a restricted motion in a square well with infinite potentials [22]. The same case can also be applied to systems in which molecules are trapped in crystalline channels or zeolites. Sekiya *et al.* [25] have also demonstrated that the molecular motions rotate around the surface of double cones. This rotational diffusion of liquid crystal molecules is a fast motion, which is accessible by means of deuterium relaxation measurements on the time scale from subnanosecond [23] to nanoseconds [22]. Moreover in the case of rotational isomerism, molecular motions about a bond in the molecules from one stable rotational isomer to another, may also occur on a time scale of picoseconds [9, 10, 12].

Both experimental [26–28] and simulation [12, 14–16] studies confirm that a polyethylene chain strongly prefers a *trans* conformation for the chain in perhydrotriphenylene or in urea crystals. Simulations [12] of molecular dynamics found that the transitions between *trans* and *gauche* states at internal $CH_2$–$CH_2$ bonds of an *n*-alkane chain are strongly suppressed by the channel of perhydrotriphenylene; these transitions are only allowed near the ends of the chain when the temperature of the simulated system is raised as high as 373 K. Simulations [14] have also shown that less than 3% of the terminal $CH_2$–$CH_2$ bonds of an *n*-alkane molecule in the urea clathrate at 300 K are in a *gauche* state at equilibrium. On the other hand, in the molecular dynamics simulations for $C_{21}$ *n*-alkane crystals [29], high correlations have been found for the (1, 3) intrachain dihedral angle pairs, arising from the sequences $g^{\pm}tg^{\mp}$, where g denotes a *gauche* state and t denotes a *trans* state. Zhan and Mattice [10] performed molecular dynamics simulations for a 1,4-*trans*-polybutadiene chain in two crystalline forms [30], i.e. form I and form II, and in the inclusion complex with perhydrotriphenylene. They found that in form I the only internal motions are fluctuations of dihedral angles at the C–C bond, and these fluctuations are smaller than those in form II or in the inclusion complex at 300 K.

On the basis of previous investigations, we can infer that the restricted motions of mesogenic molecules in liquid crystalline systems are similar to those of molecules confined in crystalline channels or in crystalline states. Molecular dynamics simulations have been successfully applied to probe the dynamics of chain molecules confined in crystalline clathrates or in crystalline states by atomistic models. Although several studies [31–34] have recently reported the simulations of liquid crystalline systems, the details of dynamical behaviour in these systems remain unclear. Therefore, we were motivated to study the dynamical behaviour of a mesogenic molecule in the smectic phases by simulations of the molecular dynamics. The equilibrated atom-based molecular models which were used to simulate the X-ray diffraction patterns, to calculate the aromatic core overlap, and to obtain the pair correlation functions for the smectic phases in our previous work [8], are adopted herein as the simulation systems.

## 2. Simulations

Molecular dynamics simulations were performed for the equilibrated models which were used to investigate the static properties of the smectics A, E and C in our previous work [8]. In brief, we developed initial models by packing mesogenic dimers with an antiparallel association into periodic boxes. Relaxed models were obtained by application of cycles of energy minimization and molecular dynamics under (NVT) conditions at 500 K on these initial states. Further molecular dynamics runs under (NPT) conditions were performed on these relaxed models at the temperature of each smectic phase [7] to obtain their equilibrated structures in the smectic phase. Fluctuations of the volumes of the systems were observed during the equilibration, and the deviations of the corresponding densities were 0.23% for the smectic A phase and 0.13% for the smectic E phase. The corrections of these models have been verified by simulated X-ray diffraction patterns [8]. Herein, the dynamic studies concentrate primarily on the equilibrated models of the smectic A and E phases. In these simulations, the dynamical behaviour was focused on the mesogenic compound (*R*)-1-methylheptyl 4[4-(2-allyloxyethoxy)-biphenyl-4′-carbonyloxy]benzoate, abbreviated as MD121B. Figure 1 depicts the chemical structure of MD121B, which contains 77 atoms (with hydrogen atoms explicitly included). This molecule is located at the centre of the simulated cells, as shown in figures 2 and 3 for the smectics A and E, respectively. The equilibrated system of the smectic A consists of 36 mesogenic molecules, with a total of 2772 discrete atoms. On the other hand, the equilibrated system of the smectic E consists of 12 mesogenic molecules and 924 discrete atoms. The sizes of unit cells were obtained from our previous work [8]. The dimensions are $a = 31.75$ Å, $b = 31.76$ Å, and $c = 34.10$ Å for smectic A, and $a = 15.95$ Å, $b = 16.28$ Å,

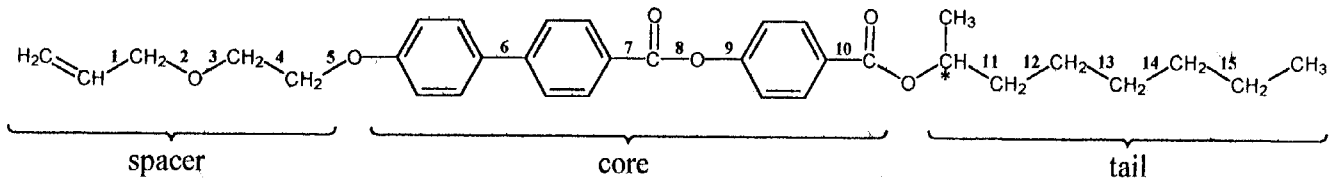


Figure 1. Chemical structure of MD121B. Calculations of the dihedral angles are dependent on the C–C or C–O bonds, which are indexed 1–15

and $c = 34.68$ Å for smectic E. To understand more thoroughly the difference in dynamical behaviour between a molecule in the bulk and an isolated molecule, we also performed a molecular dynamics simulation on an isolated MD121B molecule in a vacuum at 300 K.

The molecular dynamics simulations were carried out on a Silicon Graphics Iris Indigo workstation. The molecular dynamics trajectories were calculated with the aid of Cerius[2], as supplied by Molecular Simulations, Inc. [35]. The Dreiding II force field [36] was used for the energy calculations. The total potential energy of the system, $E_t$, was calculated from the following terms:

$$E_t = E_b + E_\theta + E_\phi + E_{inv} + E_{vdW} + E_{Coul} \quad (1)$$

where $E_b$, $E_\theta$ and $E_\phi$ are the bond stretching, bond angle bending, and dihedral angle torsion, respectively; $E_{inv}$ is the improper out-of-plane interaction, and $E_{vdW}$ and $E_{Coul}$ are the van der Waals and Coulomb interactions, respectively. All atoms in the mesogenic molecules are assigned with partial charges calculated by using the charge-equilibration algorithm [37] provided in Cerius[2].

The first four terms of equation (1) are bonded energies, and the definitions corresponding to these terms are given as follows:

$$E_b = \frac{1}{2} K_b (R - R_0)^2 \quad (2)$$

$$E_\theta = \frac{1}{2} K_\theta (\theta - \theta_0)^2 \quad (3)$$

$$E_\phi = \frac{1}{2} V_\phi \{1 - \cos[n(\phi - \phi_0)]\} \quad (4)$$

$$E_{inv} = \frac{1}{2} K_{inv} (\Psi - \Psi_0)^2 \quad (5)$$

where $K_b$, $K_\theta$ and $K_{inv}$ are the force constants for bond stretching, bond angle bending, and the inversion, respectively, and $V_\phi$ is the rotational barrier. The last two terms of equation (1) are non-bonded energies. The spline switching method [38] was applied in calculating the non-bonded interactions to reduce smoothly the interaction energies to zero by using the spline-on at 8.0 Å and the spline-off at 8.5 Å. Equation (6) shows the van der Waals non-bonded interactions through a 12-6 Lennard Jones potential,

$$E_{vdW} = D_0(\rho^{-12} - 2\rho^{-6}) \quad (6)$$

where $D_0$ is the well depth in kcal mol$^{-1}$ and $\rho = r_{ij}/r_0$, where $r_0$ is the interatomic distance in Å at which the minimum energy can be obtained, and $r_{ij}$ indicates the distance between atoms $i$ and $j$. Coulomb interactions are calculated according to

$$E_{Coul} = C_0 \sum_{i,j>i} \frac{q_i q_j}{\varepsilon r_{ij}} \quad (7)$$

where $q_i$ and $q_j$ are the charges in electron units, $r_{ij}$ is the distance in Å, $\varepsilon$ is the dielectric constant, and $E_{Coul}$ is in kcal mol$^{-1}$ when $C_0 = 332.0637$. In these simulations $\varepsilon = 1$ was used in equation (7).

In these simulations, the molecules located at the cell boundaries were fixed in space whereas the other molecules in the simulated cells were allowed to move. The molecular dynamics simulations were performed by using a canonical ensemble (constant NVT) with the Nosé thermal coupling method [39, 40]. In the molecular dynamics simulations, the time step, $\delta t = 1.0$ fs, was used to integrate the equations of motion for canonical dynamics by a leap frog Verlet algorithm [41]; the number of steps was $1.0 \times 10^6$, yielding a trajectory of 1.0 ns. The configuration of the system was recorded at intervals of 250 steps for subsequent analysis. The temperatures for the simulated systems were maintained at 393 K and at 323 K for the smectics A and E, respectively.

The dihedral angles at all of the internal C–C or C–O bonds whose indices are sequentially labelled 1–15 in the mesogenic molecule (as shown in figure 1) were monitored during the simulations. Here, the range of dihedral angle, $\phi$, is reported as either 0° to 360° or −180° to +180°, and positive angles correspond to anti-clockwise rotations. Table 1 lists the stable conformations of the dihedral angles.

## 3. Results and discussion

### 3.1. *Distributions of the dihedral angles*

The dynamical conformational behaviour of a mesogenic molecule in the smectic A or E phases can be characterized by the distributions of the dihedral

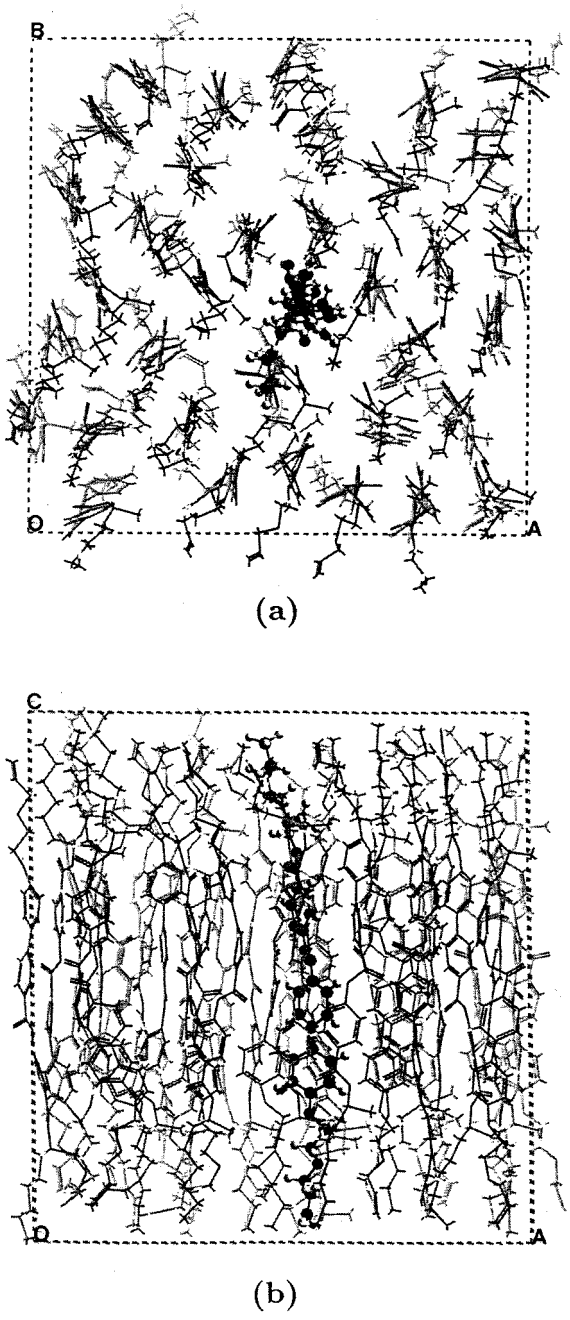


Figure 2. Equilibrated smectic A model shown in a unit cell. The mesogenic molecule is shown by a stick-ball representation. (*a*) View along the *C*-axis, (*b*) view along the *B*-axis.

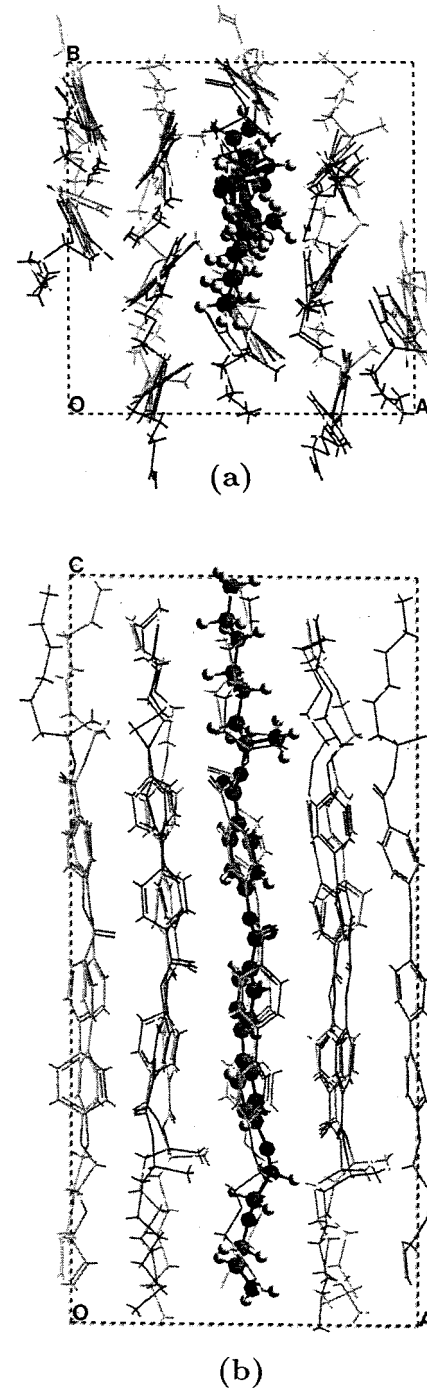


Figure 3. Equilibrated smectic E model shown in a unit cell. The mesogenic molecule is shown by a stick-ball representation. (*a*) View along the *C*-axis, (*b*) view along the *B*-axis.

angles; these are compared with those of an isolated molecule simulated in vacuum. This comparison can give indications of the effect of molecular packing in the liquid crystalline states. Figures 4 and 5 show the distributions of the dihedral angles, each averaged over a trajectory of 1.0 ns, at 15 internal C–C or C–O bonds in the MD121B molecule, in the smectic A phase at 393 K and in the smectic E phase at 323 K, respectively. Panels (*a*), (*b*), and (*c*) in figures 4 and 5 show the distributions of the dihedral angles for the spacer, core, and tail, respectively. These distributions, except for the bond indexed by 1 in figure 4(*a*) and for the bond

Table 1. Stable conformations of the dihedral angles.

| Placements | Abbreviation | Dihedral angle/deg |
|---|---|---|
| *Cis* | c | 0 (360) |
| *Trans* | t | 180 |
| *Gauche*$^+$ | $g^+$ | 60 |
| *Gauche*$^-$ | $g^-$ | − 60 (300) |
| *Anticlinal*$^+$ | $a^+$ | 120 |
| *Anticlinal*$^-$ | $a^-$ | − 120 (240) |

indexed by 2 in figure 5 (*a*), all have a similar appearance, showing a single Gaussian-like distribution. As shown in figure 4 (*a*), the distribution of the dihedral angle at the bond CH–$CH_2$, indexed by 1, shows two stable conformations with an absolute value of ∼60° from the *trans* state. According to table 1, these stable conformations can be assigned as an anticlinal state, because the anticlinal conformation has a preference for occurring at the CH–$CH_2$ bond, which is linked to $H_2C$=CH. In contrast, the distribution at the bond indexed by 1 shown in figure 5 (*a*), is restricted to the *trans* state. However, the shape of this distribution is broad Gaussian-like; this restricted motion may enforce a transition close to the $g^+$ state at the bond indexed by 2 in figure 5 (*a*).

In order to facilitate a comparison, figure 6 displays the corresponding distributions of the dihedral angles for an isolated MD121B molecule, as calculated in vacuum at 300 K. Figures 6 (*a*), 6 (*b*), and 6 (*c*) present the distributions for the spacer, core, and tail, respectively. The distribution of the dihedral angle at the bond indexed by 1 is that occurring at the bond attached to $H_2C$=CH. Therefore, as shown in figure 6 (*a*), it clearly indicates that there are two anticlinal conformations with an absolute value of ∼60° from the *trans* state. The distributions of the dihedral angles at the bonds indexed by 2, 3, and 5 have $g^+$, *trans*, and $g^-$ rotational isomeric state transitions; that at the bond indexed by 4 has only a *trans* conformation. Here, the most probable conformations for *trans* are located at 180°, for $g^+$ at 75°, and for $g^-$ at 280°. In addition, all distributions have a higher value of probability at the *trans* state than any other states. For the core, as shown in figure 6 (*b*), the distribution of the dihedral angle at the bond indexed by 6, which is located between two phenyl rings, is split into two peaks: one is centred at 60° ($g^+$), the other at 120° ($a^+$). Ishaq *et al.* [42] have indicated that there are four minima at ±53° and ±127° for the dihedral angle located between two phenyl rings, and a low energy barrier between the states at + 53° and + 127° or at − 53° and − 127°. Thus, this distribution centred at 60° and 120° for bond 6 is correlated well with the minima at + 53° and + 127°. For the bonds indexed by 7, 8, and 10, the distributions of the dihedral angles are

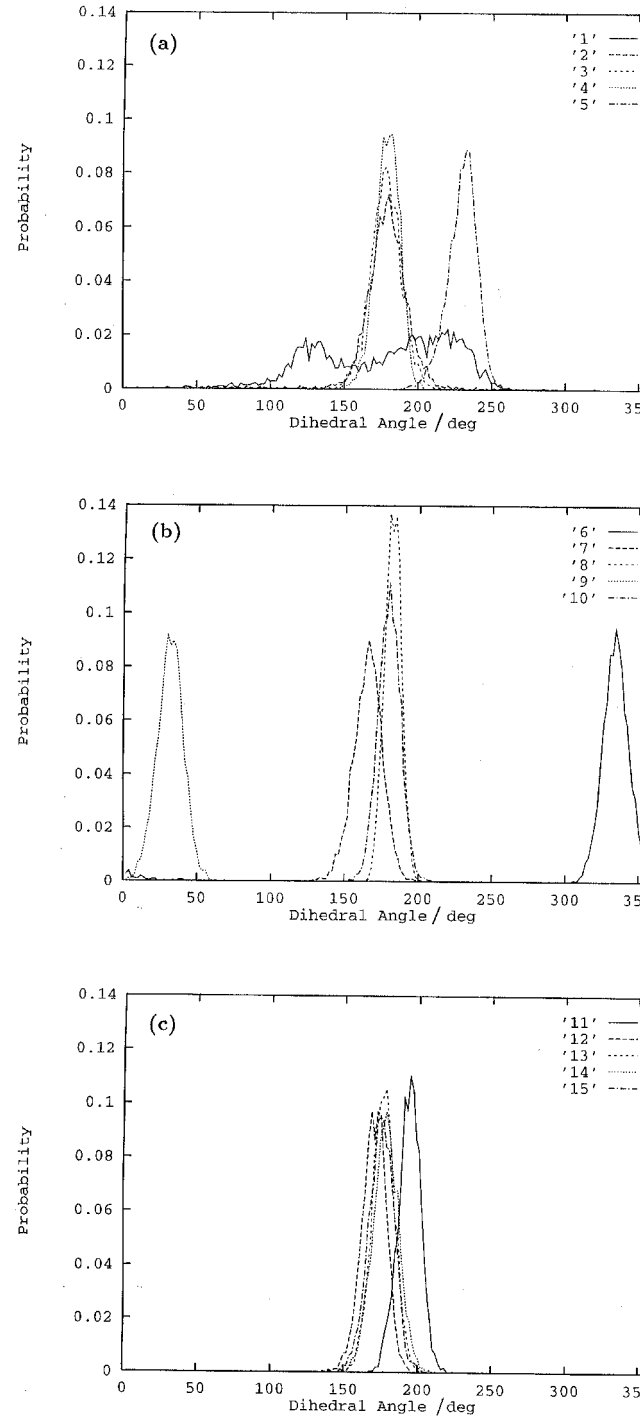


Figure 4. Distribution of the dihedral angles at the internal C–C or C–O bonds in the mesogenic molecule in the smectic A at 393 K, evaluated over a 1.0 ns trajectory. The indices for the C–C or C–O bonds correspond to those shown in figure 1. (*a*) Spacer, (*b*) core and (*c*) tail.

centred at 180°, which is at the *trans* conformation; the distribution at the bond indexed by 9 is centred at 0°, which is at the *cis* conformation. For the tail, as shown

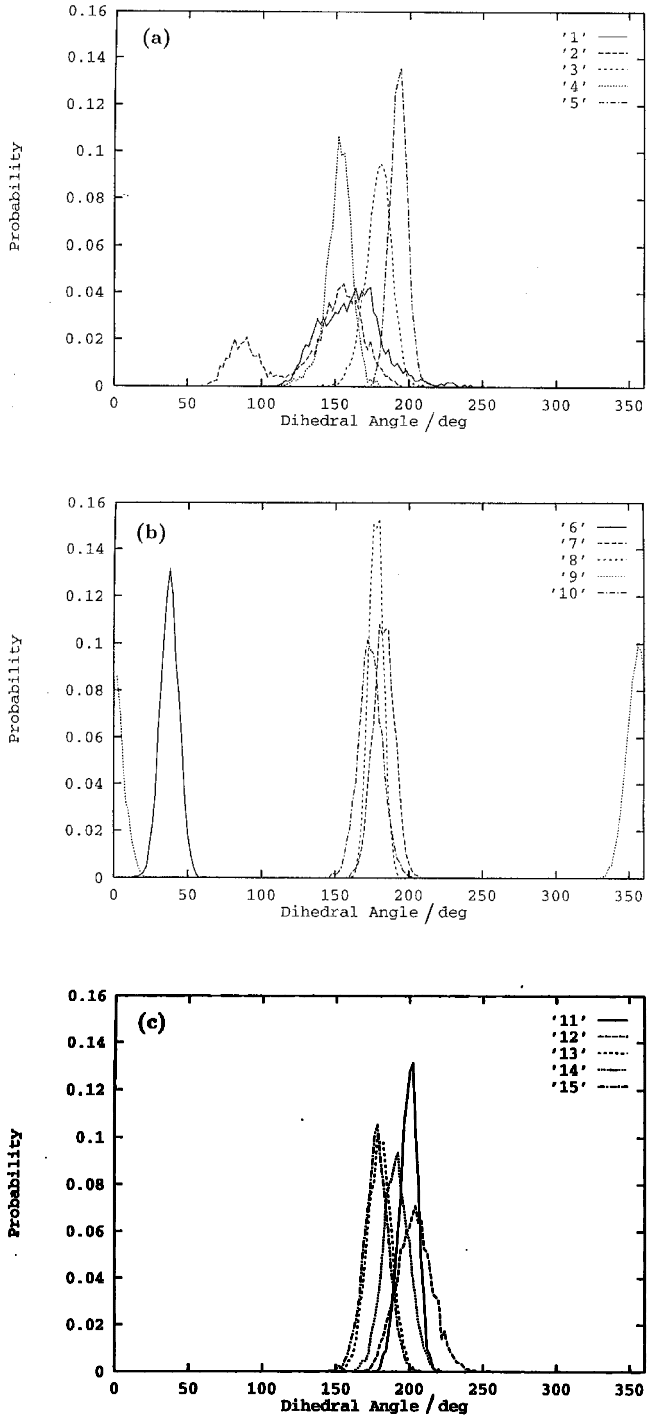


Figure 5. Distribution of the dihedral angles at the internal C–C or C–O bonds in the mesogenic molecule in the smectic E at 323 K, evaluated over a 1.0 ns trajectory. The indices for the C–C or C–O bonds correspond to those shown in figure 1. (*a*) Spacer, (*b*) core, (*c*) tail.

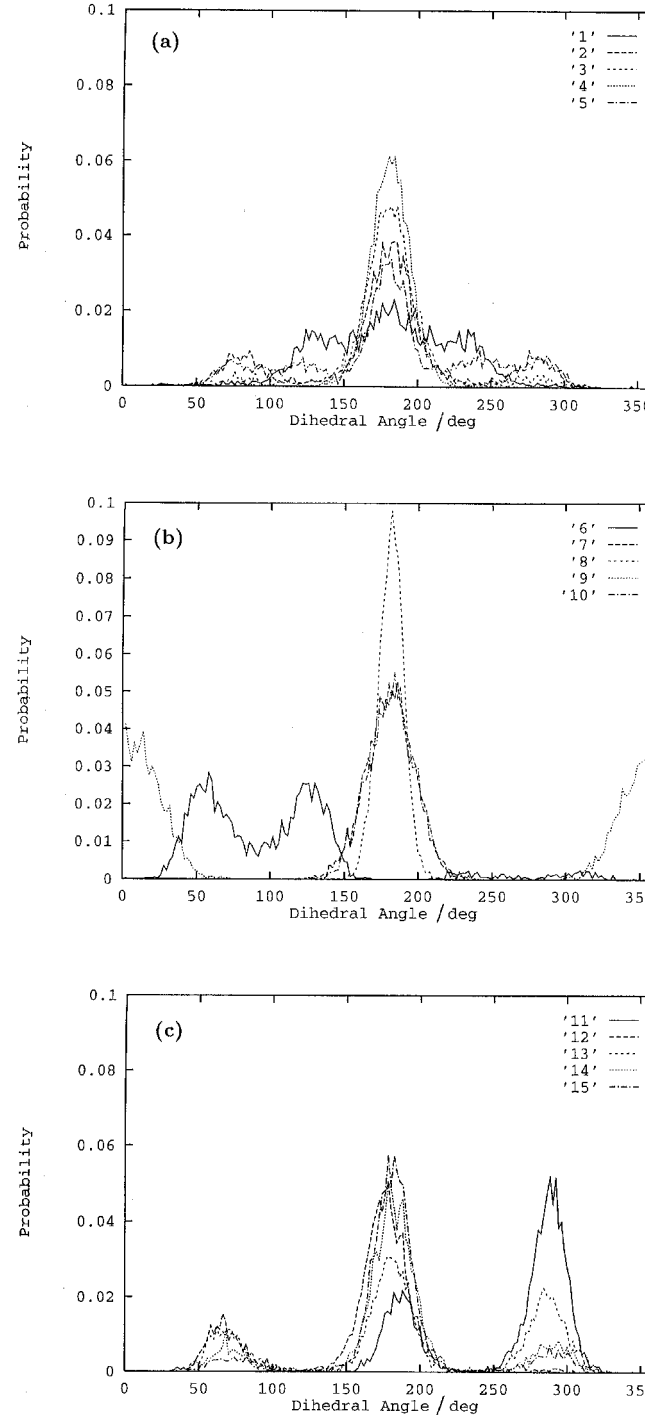


Figure 6. Distribution of the dihedral angles at the internal C–C or C–O bonds in the mesogenic molecule in a vacuum at 300 K, evaluated over a 1.0 ns trajectory. The indices for the C–C or C–O bonds correspond to those shown in figure 1. (*a*) Spacer, (*b*) core, (*c*) tail.

in figure 6(*c*), the distribution of the dihedral angle at the bond labelled 11 has two peaks: one is the *trans* conformation and the other is the $g^-$ conformation; the value of probability is higher for the $g^-$ state than for the *trans* state. The methyl group, which is connected to the chiral centre C*, produces an unsymmetrical

arrangement, so that there is no $g^+$ conformation at the bond labelled 11. On the other hand, because the distribution of the dihedral angle at the bond indexed 12 is affected by the bond labelled 11, there are two rotational isomeric states occurring at this bond, i.e. *trans* and $g^+$, but there is no $g^-$. In addition, the value of probability is higher for the *trans* state than for the $g^+$ state. However, the distributions of the dihedral angles at the bonds labelled 13, 14, and 15, all exhibit the same trend that has the appearance of rotational isomeric state transitions, such as $g^+$, *trans*, and $g^-$ conformations. Among these distributions, the *trans* conformation has the highest value of probability.

In summary, figure 6 depicts the transitions between rotational isomeric states at bonds in the isolated molecule simulated in a vacuum at 300 K, and these transitions are either from the *trans* to $g^{\pm}$ states or from the *trans* to $a^{\pm}$ states except for the bond labelled 4 and for the bonds in the core. Figures 4 and 5 indicate that, except for the bond labelled 1 in figure 4(*a*) and for the bond labelled 2 in figure 5(*a*), no rotational isomeric state transitions were observed at the bonds in the molecule in the smectics A and E. Comparing figures 4 and 5 with figure 6 reveals that the distributions of the dihedral angles strongly favour a *trans* conformation in the smectics A and E. Such a tendency implies that the internal motions of the dihedral angles at the bonds in the molecule are restricted in the smectics A and E. These restrictions are similar to those of *n*-alkane molecules confined in crystalline channels [12, 14–16].



### 3.2. *Fluctuations of dihedral angles*

The internal motions of the dihedral angles can be represented by fluctuations of each dihedral angle about its mean value. The magnitude, $\delta\phi$, of the fluctuations of a dihedral angle calculated in the smectic A phase, in the smectic E phase, or in a vacuum is formulated as

$$\delta\phi = (\langle \phi^2 \rangle - \langle \phi \rangle^2)^{1/2} \quad (8)$$

where the angle brackets denote the statistical averages of the enclosed quantity. Tables 2, 3, and 4 list the values of $\delta\phi$ and $\langle \phi \rangle$ for the states in the smectics A and E as well as for the state in a vacuum, respectively, during a trajectory of 1.0 ns. They include the absolute values of $\langle \phi \rangle - \phi_t$, where $\phi_t$ denotes the dihedral angle for a *trans* conformation. A value of $\delta\phi$ represents the breadth of fluctuations for a dihedral angle. A mean value in $\langle \phi \rangle$ denotes the precise location of the most probable appearance of a dihedral angle. The values of $\delta\phi$ in tables 2 and 3 indicate that most of the bonds in the spacer and core fluctuate more in the smectic A than in the smectic E. On the other hand, the fluctuations at the bonds in the tail in the smectics A and E are comparable. Furthermore, the values of $\delta\phi$ in tables 2 and 3 also show that the fluctuations are higher at the bonds in the spacer than those at the bonds in the tail in both smectics A and E. Therefore, the spacer and tail are denoted as 'soft' and 'hard' segments, respectively, in this work.

Table 2. Fluctuations and mean values of the dihedral angles at the bonds in MD121B in the smectic A phase (deg).

| Part | Index[a] | $\delta\phi$ | $\langle \phi \rangle$ | $\lvert\langle \phi \rangle - \phi_t\rvert$ |
|---|---|---|---|---|
| Spacer | 1 | 44.9 | 177.4 | 2.6 |
| | 2 | 16.3 | 177.8 | 2.2 |
| | 3 | 10.7 | 176.9 | 3.1 |
| | 4 | 8.3 | 178.1 | 1.9 |
| | 5 | 10.0 | 228.6 | 48.6 |
| Core | 6 | 10.2 | 334.3 | 154.3 |
| | 7 | 9.7 | 164.7 | 15.3 |
| | 8 | 5.6 | 181.3 | 1.3 |
| | 9 | 8.8 | 30.9 | 149.1 |
| | 10 | 7.6 | 179.0 | 1.0 |
| Tail | 11 | 7.6 | 193.0 | 13.0 |
| | 12 | 8.3 | 169.2 | 10.8 |
| | 13 | 7.6 | 175.4 | 4.6 |
| | 14 | 8.8 | 177.1 | 2.9 |
| | 15 | 8.5 | 174.1 | 5.9 |

[a] Indices of the bonds corresponding to those shown in figure 1.

Table 3. Fluctuations and mean values of the dihedral angles at the bonds in MD121B in the smectic E phase (deg).

| Part | Index[a] | $\delta\phi$ | $\langle \phi \rangle$ | $\lvert\langle \phi \rangle - \phi_t\rvert$ |
|---|---|---|---|---|
| Spacer | 1 | 21.2 | 160.0 | 20.0 |
| | 2 | 31.8 | 136.3 | 43.7 |
| | 3 | 8.9 | 178.1 | 1.9 |
| | 4 | 9.0 | 151.4 | 28.6 |
| | 5 | 6.0 | 191.7 | 11.7 |
| Core | 6 | 6.3 | 36.7 | 143.3 |
| | 7 | 7.2 | 181.9 | 1.9 |
| | 8 | 4.9 | 176.7 | 3.3 |
| | 9 | 8.0 | 355.8 | 175.8 |
| | 10 | 8.2 | 173.0 | 7.0 |
| Tail | 11 | 6.3 | 198.2 | 18.2 |
| | 12 | 12.1 | 202.6 | 22.6 |
| | 13 | 8.1 | 178.4 | 1.6 |
| | 14 | 9.1 | 190.0 | 10.0 |
| | 15 | 8.5 | 176.4 | 3.6 |

[a] Indices of the bonds corresponding to those shown in figure 1.

The criterion of low values of $\delta\phi$ and $|\langle \phi \rangle - \phi_t|$ must be satisfied for bonds, that are restricted to the region of the *trans* conformation in the smectics A and E. As tables 2 and 3 reveal, the bonds confined in the *trans* state are those indexed by 2, 3, 4, 7, 8, and 10, as well as the bonds in the tail for the smectic A; those bonds

Table 4. Fluctuations and mean values of the dihedral angles at the bonds in MD121B in vacuum (deg).

| Part | Index[a] | $\delta\phi$ | $\langle\phi\rangle$ | $\lvert\langle\phi\rangle - \phi_t\rvert$ |
|---|---|---|---|---|
| Spacer | 1 | 43.9 | 180.0 | 0.0 |
| | 2 | 55.1 | 180.0 | 0.0 |
| | 3 | 33.9 | 181.0 | 1.0 |
| | 4 | 16.1 | 180.1 | 0.1 |
| | 5 | 58.1 | 183.9 | 3.9 |
| Core | 6 | 55.5 | 101.0 | 79.0 |
| | 7 | 16.5 | 180.1 | 0.1 |
| | 8 | 8.8 | 180.4 | 0.4 |
| | 9 | 21.0 | 361.1 | 181.1 |
| | 10 | 15.9 | 180.8 | 0.8 |
| Tail | 11 | 47.5 | 256.0 | 76.0 |
| | 12 | 46.7 | 155.8 | 24.2 |
| | 13 | 76.2 | 195.0 | 15.0 |
| | 14 | 54.5 | 183.5 | 3.5 |
| | 15 | 43.8 | 183.6 | 3.6 |

[a] Indices of the bonds corresponding to those shown in figure 1.

indexed by 3, 5, 7, 8, 10, 11, 13, 14, and 15 apply to the smectic E.

According to table 4, the large values of $\delta\phi$ at the bonds in the isolated molecule simulated in a vacuum suggest that these bonds experience not only *trans* conformation but also $g^{\pm}$ conformations. The low values of $|\langle\phi\rangle - \phi_t|$ in table 4 imply that the transitions between rotational isomeric states have a symmetry about $\phi_t$. However, the large values of $|\langle\phi\rangle - \phi_t|$ at bonds indexed by 6 and 9 arise because the shape of the distributions of the dihedral angles (figure 6) is unsymmetrical about $\phi_t$. Moreover, the large values of $|\langle\phi\rangle - \phi_t|$ at bonds indexed by 11 and 12 are due to intramolecular interactions with the methyl group at the chiral centre, causing unsymmetrical fluctuations about $\phi_t$. The fluctuations of the dihedral angles at the bonds indexed by 4, 7, 8, and 10 in table 4 are restricted in the *trans* state. These restricted fluctuations are the result of small values of $\delta\phi$ and $|\langle\phi\rangle - \phi_t|$ that are found at these bonds.

### 3.3. *Transitions of the dihedral angles*

Transitions of the dihedral angles at all of the internal C–C or C–O bonds in the mesogenic molecule were observed during the simulations. Here, the observations of the transitions focused on the smectic A phase. Figures 7(*a*), 7(*b*), and 7(*c*) record the instantaneous values of the dihedral angles at the 15 internal C–C or C–O bonds in the mesogenic molecule in the smectic A during a trajectory of 1.0 ns at 393 K for the spacer, core, and tail, respectively. Index 1 in figure 7(*a*) depicts the history of the dihedral angle at the bond CH–$CH_2$. As this history reveals, there is a high frequency of transitions between 50° and 250°. Here, the history displays a high density at $a^+$ (120°) or at $a^-$ (220°), showing rotational isomeric state transitions between $a^{\pm}$ states at the CH–$CH_2$ bond. Index 2 in figure 7(*a*) depicts the history of the dihedral angle at the $CH_2$–O bond. This history denotes an extremely brief transition for about 8 ps duration from the *trans* state to the $g^+$ state at 710 ps, and several large fluctuations away from the *trans* state. Rotational isomeric state transitions are different from fluctuations about a mean value by lasting for the duration of a stable state. The rotational isomeric state transitions involve initial and final states that remain stable for at least 5 ps [10]. Other bonds, which are indexed by 3–15, experience no rotational isomeric state transitions; however rapid fluctuations of the dihedral angles with respect to their most probable values can be found in figures 7(*a*), 7(*b*), and 7(*c*).

Figures 7(*a*), 7(*b*), and 7(*c*) plot 15 dihedral angle histories, each containing 4000 instantaneous values of a dihedral angle, which cover a trajectory of 1.0 ns. These 4000 values were grouped into 180 equal intervals, each having a value of 2°. Plots of the proportion of the values occurring in each interval as a function of the values of a dihedral angle directly give a dihedral angle distribution. Therefore, the plots in figures 7(*a*), 7(*b*), and 7(*c*) can be converted into the corresponding dihedral angle distributions, as shown in figures 4(*a*), 4(*b*), and 4(*c*).

As depicted in figures 7(*a*), 7(*b*), and 7(*c*), it is much clearer to show the fluctuations of the dihedral angles than these fluctuations quantified by $\delta\phi$, as shown in table 2. If the fluctuations of the dihedral angles in the spacer, figure 7(*a*), are compared with those in the tail, figure 7(*c*), the dihedral angles in the spacer can easily be found to experience greater fluctuations than those in the tail. These larger fluctuations imply more disorder in the spacer than in the tail of the mesogenic molecule. Such a difference is readily apparent if the values of fluctuations at the bond indexed by 1 are compared with those at the bond indexed by 15. This observation corresponds to the values of $\delta\phi$, as shown in tables 2 and 3, which indicate that the spacer is a 'soft' segment and the tail a 'hard' segment in the mesogenic molecule.

### 3.4. *Dihedral angles fluctuating between the lower and upper limits*

Intermolecular interactions in the core of the molecule are of critical concern since they govern the transitions either between the smectic phases or from the smectic to isotropic phases. Here, the fluctuations of the dihedral angles, whose deviations fall within the lower and upper limits, are focused on the core. The lower and upper limits are based on the maximum fluctuations of a dihedral angle with respect to its mean value; they are taken from the lowest values of probability, which

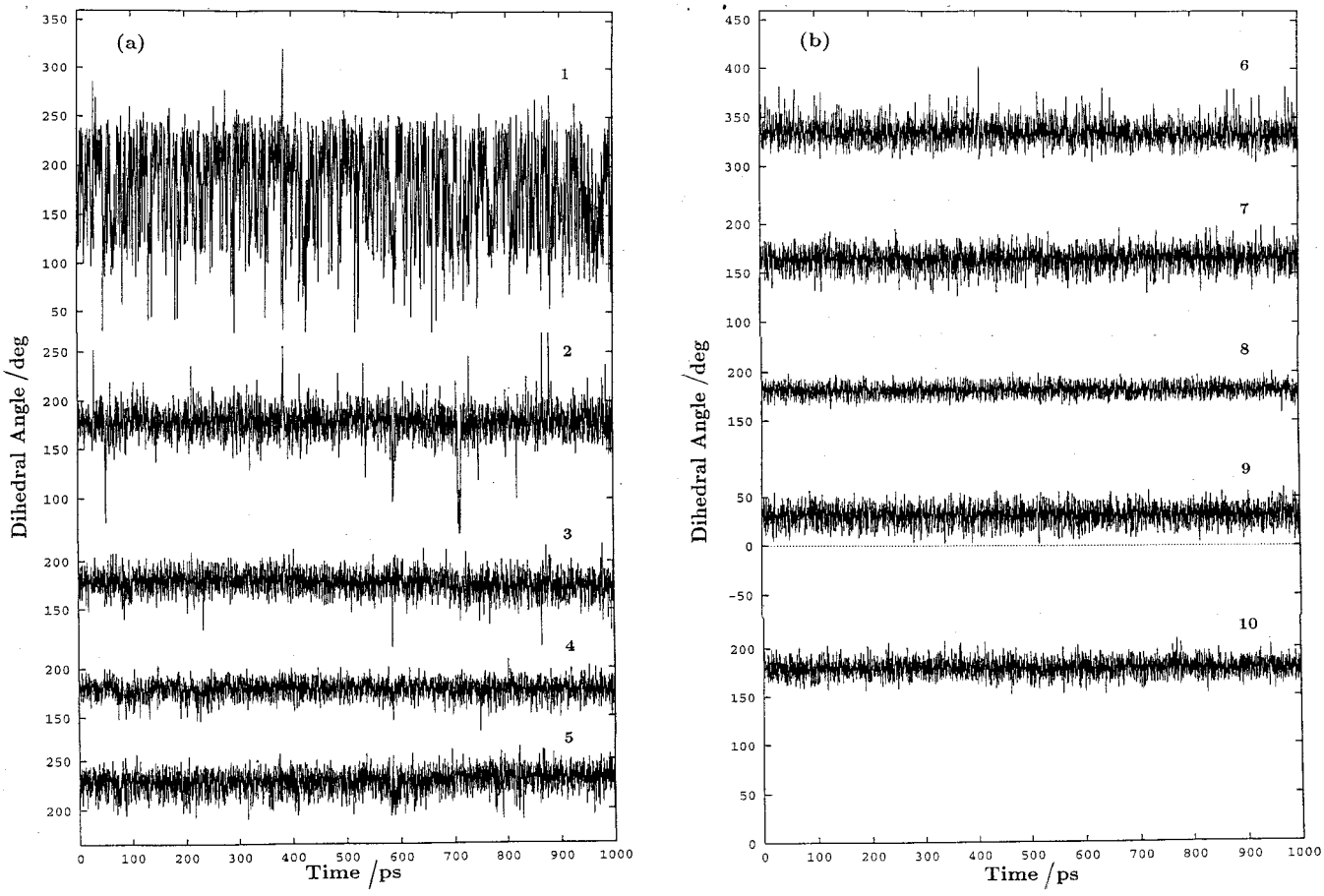


Figure 7. History of the dihedral angles at the internal C–C or C–O bonds in the mesogenic molecule in the smectic A at 393 K, evaluated over a 1.0 ns trajectory. Indices correspond to those shown in figure 1. (*a*) Spacer, (*b*) core, (*c*) tail.



are located on both sides of the distribution of a dihedral angle. The results are summarized in table 5 in which the range of a dihedral angle is represented as − 180° to + 180°.

In order to facilitate comparisons of the results listed in table 5 with those of our previous work [8], we also show the results of AM1 calculations. On the basis of AM1 calculations, the dihedral angles at the bonds in the core can be classified into two categories: one is near the *cis* conformation, such as the bonds indexed by 6 and 9, and the other is centred at the *trans* conformation, such as the bonds indexed by 7, 8, and 10. Rows 2 and 3 in table 5 list the values of the dihedral angles for the lower and upper limits, respectively, as evaluated from figure 4(*b*). Figure 5(*b*) provides the values in rows 4 and 5 of table 5; figure 6(*b*) provides the values in rows 6 and 7. Interestingly, the dihedral angles fluctuating between the lower and upper limits fall within the corresponding quadrants that are occupied by the favourable values obtained from AM1 calculations. As table 5 clearly reveals, the bonds labelled by 6 and 9 strongly prefer the dihedral angles fluctuating in quadrants I and IV, except that the dihedral angle at the bond indexed by 6 in vacuum fluctuates beyond quadrant I. On the other hand, the bonds indexed by 7, 8, and 10 strongly favour the dihedral angles fluctuating in quadrants II and III.

### 3.5. *Rotational diffusion of the mesogenic molecule*

Rotational motions of a molecule around its long axis were represented by using a polar coordinate system [10, 12, 14] with the $Z$ axis parallel to the $C$ axis of the simulated cell. Here, we adopt the polar coordinate system to describe rotational diffusion of the mesogenic molecule. The instantaneous value of the angle between the $Z$ axis and a selected bond vector in the mesogenic molecule is denoted by $\theta$. For example, $\theta = 0°$, 90°, and 180° when the bond vector is parallel, perpendicular, or antiparallel to the $Z$ axis. The rotation of the selected bond vector about the $Z$ axis is denoted by $\psi$, which was obtained by projecting the selected bond vector onto the $XY$ plane. Thus, the value of $\psi$ shows the orientation of the selected bond vector from the mesogenic molecule in the coordinate defined by the simulated

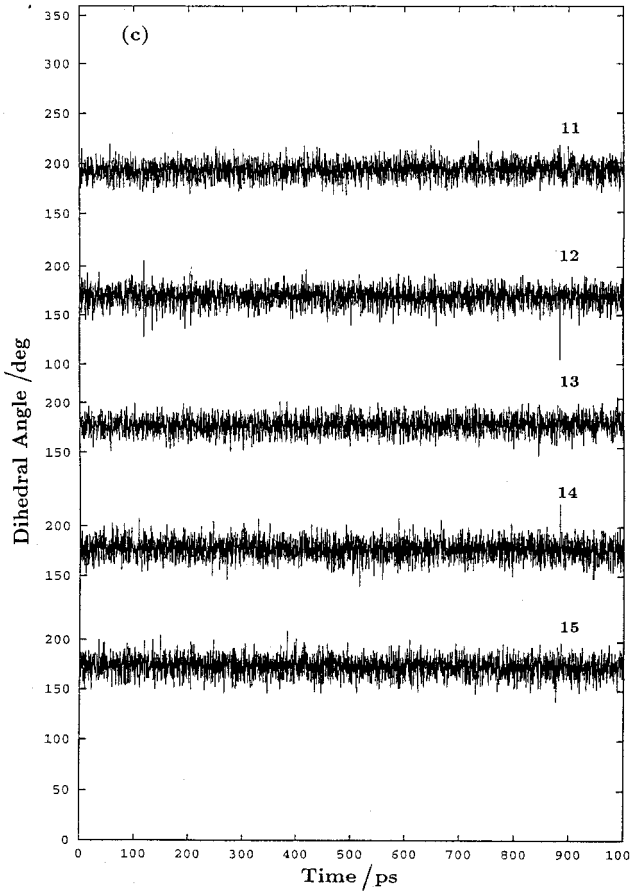


Figure 7. (*continued*).

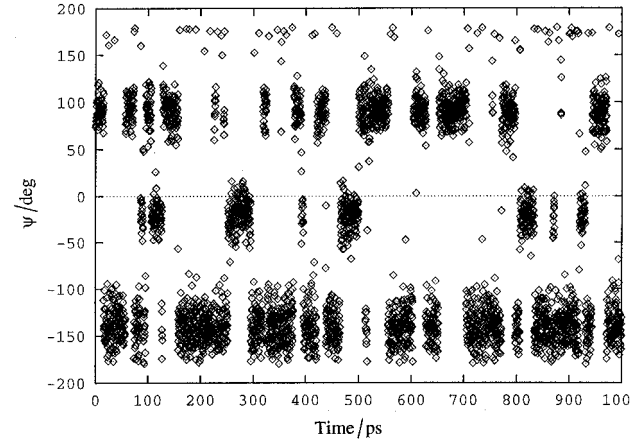


Figure 8. Orientation of the projection of a selected C–H bond vector in the terminal methyl group of the tail onto the $XY$ plane in the smectic A at 393 K for a trajectory of 1.0 ns.

cell. The values of $\theta$ and $\psi$ were recorded at intervals of 0.25 ps over a trajectory of 1.0 ns. Figure 8 shows the values of $\psi$ obtained from the projection of a selected C–H bond vector in the terminal $-CH_3$ group of the tail part in the MD121B molecule, located at the centre of the simulated cell (figure 2) in the smectic A phase, onto the $XY$ plane during a trajectory of 1.0 ns. The values of $\psi$ can be affected by three factors: (1) rotation of the molecule about its long axis, (2) fluctuations in the dihedral angles at C–C or C–O bonds, and (3) bond-bending modes. The angle plotted in figure 8 is obtained from the value between the $X$ axis and the projection of a selected C–H bond onto the $XY$ plane. As shown in figure 8, it is clear that the orientation of the C–H bond vector is favourable in three regions. Also, figure 8 reflects a slight preference of two orientations over one orientation. Figure 9(*a*) depicts the values of $\psi$ as shown in figure 8 by a polar coordinate system. The instantaneous value of $\theta$ determines the radial distance from the centre of the figure to points; in addition, $\psi$ determines the angle with the solid line.

Figure 9(*a*) illustrates the correlation between $\theta$ and $\psi$. Instantaneous values of $\theta_x$ and $\theta_y$ are determined from equations (9) and (10):

$$\theta_x = \theta \cos(\psi) \tag{9}$$

$$\theta_y = \theta \sin(\psi). \tag{10}$$

Table 5. Dihedral angles fluctuating between the lower and upper limits in the core (deg).

| Origin | Limit | 6 | 7 | 8 | 9 | 10 |
|---|---|---|---|---|---|---|
| AM1[a] | | ~ ±40 | ~ ±175 | ~ ±178 | ~ ±40 | ~ ±179 |
| SmA[b] | Lower | − 45.0 | − 175.0 | − 165.0 | 10.0 | − 165.0 |
| | Upper | 5.0 | 140.0 | 170.0 | 50.0 | 165.0 |
| SmE[c] | Lower | 20.0 | − 160.0 | − 170.0 | − 25.0 | − 165.0 |
| | Upper | 55.0 | 160.0 | 165.0 | 20.0 | 150.0 |
| Vacuum[d] | Lower | 25.0 | − 145.0 | − 160.0 | − 50.0 | − 140.0 |
| | Upper | 150.0 | 140.0 | 160.0 | 50.0 | 140.0 |

[a] Values obtained from previous work [8] by using AM1 calculations.
[b] Values obtained from figure 4(*b*).
[c] Values obtained from figure 5(*b*).
[d] Values obtained from figure 6(*b*).

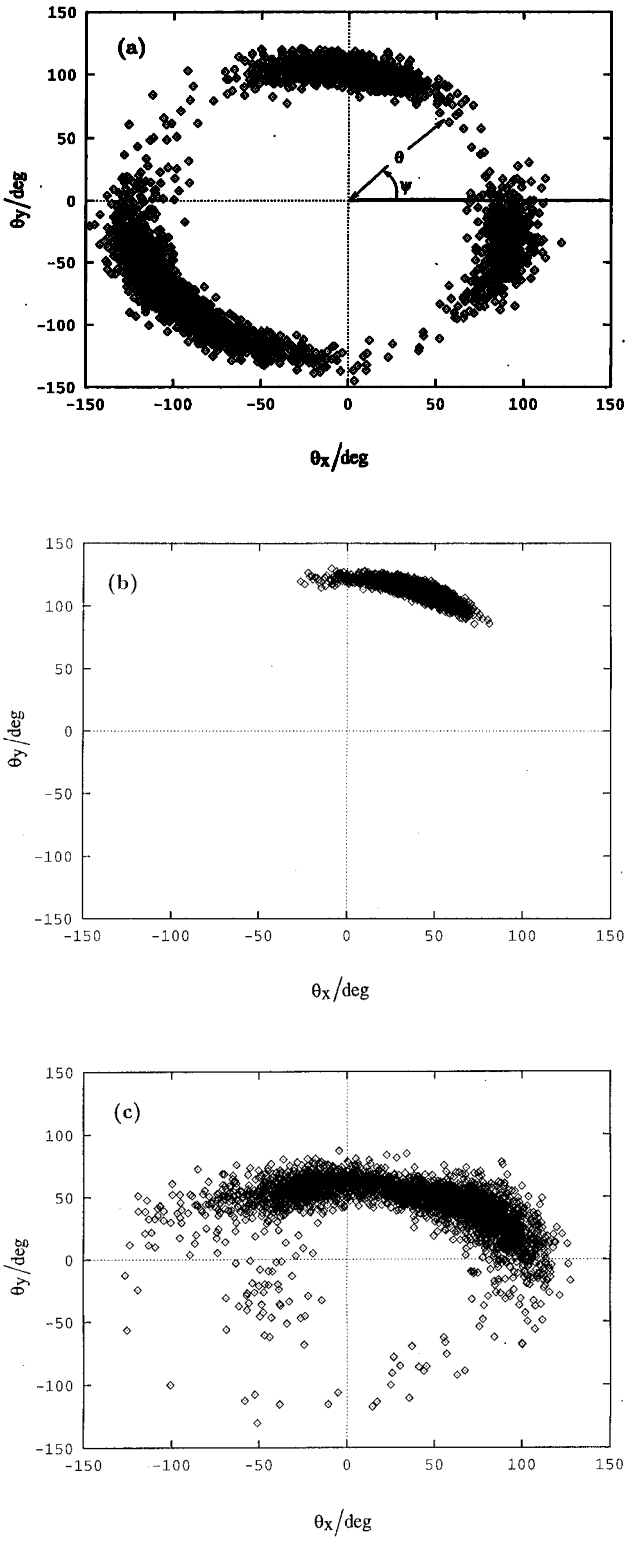


Figure 9. Angular distribution for $\psi$ and $\theta$ for a selected bond vector in the tail, core, or spacer of the mesogenic molecule in the smectic A during 1.0 ns at 393 K. (*a*) C–H bond vector in the terminal methyl group of the tail, (*b*) C=O bond vector located between diphenyl and phenyl groups in the core, and (*c*) C–H bond vector in the $CH_2$= group of the spacer.

Figure 9(*b*) shows the record of the values of $\theta$ and $\psi$ for the C=O bond vector, which is located between the bonds indexed by 7 and 8, in the core of the molecule in the smectic A phase; figure 9(*c*) presents the record for a particular C–H bond vector in the $CH_2$= group in the spacer. Figures 10(*a*), 10(*b*), and 10(*c*) display the angular distributions of rotational diffusion for the MD121B molecule located at the centre of the simulated cell (figure 3) in the smectic E for the tail, core, and spacer, respectively. These angular distributions correspond to those shown in figures 9(*a*), 9(*b*), and 9(*c*).

Figures 9(*a*) and 10(*a*) show that the density of points is not uniform over the entire range of $\psi$. The values of $\psi$ in figure 9(*a*) are taken from figure 8; they prefer three relatively broad ranges: $45° < \psi < 125°$, $-60° < \psi < +15°$, and $-185° < \psi < -85°$. The values of $\psi$ in figure 10(*a*) also have a similar appearance, governed by three broad ranges, such as $50° < \psi < 120°$, $-60° < \psi < +5°$, and $-170° < \psi < -110°$. Hence, the values of $\psi$ obtained from figures 9(*a*) and 10(*a*) all have three preferred occupancies that may reflect the C–H bond vector in the terminal methyl group having three preferences of orientation. To understand these results, it is useful to examine the distributions of the dihedral angle at the last C–C bond in the terminal $-CH_2-CH_3$ group of the molecule. Figures 11(*a*) and 11(*b*) show the transitions of the dihedral angle at the last C–C bond in the tail part of the molecule in the smectics A and E, respectively. Figure 11 indicates that rotational isomeric state transitions occur in three preferred states evidenced by high values of probability; these states are $g^+$, *trans*, and $g^-$.

Figures 9(*b*) and 10(*b*) show that the density of points is uniform and narrow over the entire range of $\psi$ for the core of the molecule. The values of $\psi$, as shown in figure 9(*b*), are located in a range between 50° and 100°, and those evaluated from figure 10(*b*) are between 98° and 128°. Such angular distributions in a uniform and narrow range may reflect the C=O bond vector having a preference for one orientation in the core. As shown in previous sections, the fluctuations of the dihedral angles at the bonds in the core of the molecule in the smectics A and E are confined either near the *cis* state or in the *trans* state. Thus, these arrangements suggest that the core part of the molecule is nearly coplanar, facilitating favourable intermolecular interactions. This tendency towards a uniform and narrow range of rotational diffusion may be due to these intermolecular interactions.

Figures 9(*c*) and 10(*c*) demonstrate that the density of points is uniform and broad over the entire range of $\psi$. The values of $\psi$ from figure 9(*c*) prefer the range between $-50°$ and 175°. Those values adopted from figure 10(*c*) are located in the range between 80° and

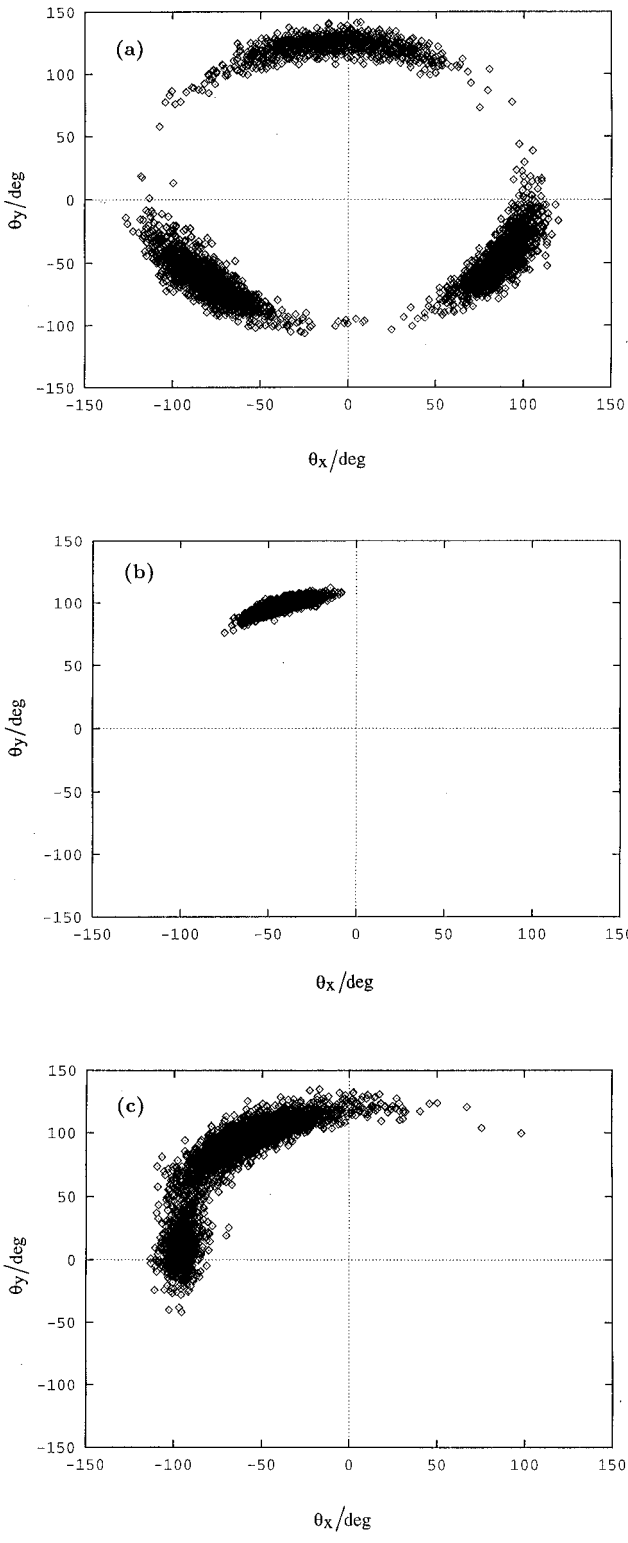


Figure 10. Angular distribution for $\psi$ and $\theta$ for a selected bond vector in the tail, core, or spacer of the mesogenic molecule in the smectic E at 323 K. (*a*) C–H bond vector in the terminal methyl group of the tail, (*b*) C=O bond vector located between diphenyl and phenyl groups in the core, and (*c*) C–H bond vector in the $CH_2$= group of the spacer.

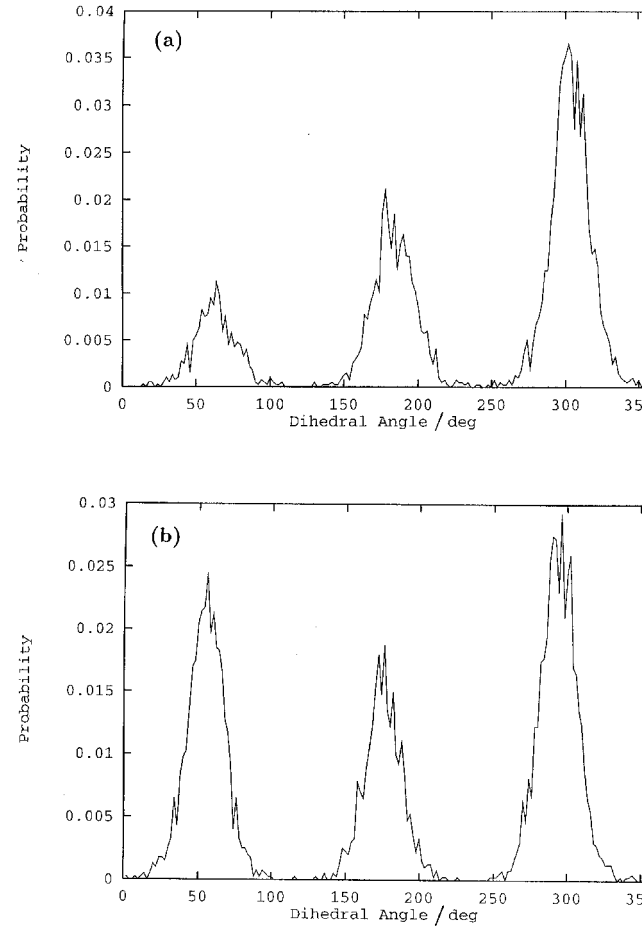


Figure 11. Distribution of the dihedral angle at the last C–C bond of the terminal –$CH_2$–$CH_3$ group in the tail of the mesogenic molecule, evaluated over a 1.0 ns trajectory. (*a*) In the smectic A at 393 K, (*b*) in the smectic E at 323 K.

190°. The values of $\psi$ in these figures imply that the C–H bond vector in the $CH_2$= group of the spacer has a strong tendency to a preference of orientations, since there are no rotational isomeric state transitions that can be observed at this terminal double bond. Furthermore, it has more librational motion than that observed at the C=O bond vector in the core. This is because the C–H bond vector in the $CH_2$= group possesses a broad range of angular distributions.

Comparing the corresponding parts of figures 9 and 10 reveals that the density of points is denser in figure 10 than in figure 9. Therefore, the molecule in the smectic A phase is more mobile than that in the smectic E phase. Moreover, as shown in figures 9 and 10, it is apparent that the ranges of the angular distributions are broader at the ends than in the middle of the molecule. Therefore, one can infer that rotational diffusion observed at the bond vectors in the mesogenic molecule, about the axis defined by the simulated cells, is greater at the ends than

in the middle of the molecule in either the smectic A phase or the smectic E phase. This type of motion suggests that the molecule would undergo rotational diffusion around its long axis in a manner similar to that seen in previous investigations [20, 22]; i.e. using a square well with infinite potentials to account for rotational diffusion of molecules in a cone model in thermotropic liquid crystals.

## 4. Conclusions

We have studied the molecular dynamics of the MD121B molecule, which has been investigated in our previous works [7, 8], in the smectic A and E phases, as well as in a vacuum, by using molecular dynamics simulations. These simulations suggest that the shape of the distributions of the dihedral angles at the bonds in this molecule in the smectics A and E has an appearance close to a Gaussian-like distribution, except for the bonds near the end of the spacer segment. This Gaussian-like distribution implies not only that no rotational isomeric state transitions occur at these bonds, but also that the internal motions at these bonds are restricted during the trajectory of 1.0 ns. The principal motions of this dynamical study are the fluctuations of the dihedral angles with respect to their mean values at the C–C or C–O bonds in the smectic A at 393 K or in the smectic E at 323 K. These fluctuations are smaller in $\delta\phi$ than the corresponding fluctuations in vacuum at 300 K. One criterion has been used to determine the fluctuations of the dihedral angles that are restricted in the *trans* state. This criterion is that the values of $\delta\phi$ and $|\langle\phi\rangle - \phi_t|$ are small. Moreover, based on the history of dihedral angles, the fluctuations of the dihedral angles in the spacer segment are apparently larger than those of the dihedral angles in the tail segment of the molecule. This finding may suggest not only that the spacer is a 'soft' segment but also that the tail is a 'hard' segment. Rotational diffusion of the mesogenic molecule was obtained by observing the rotations of the C–H bond vectors at the ends of the molecule or the C=O bond vector in the middle of the molecule with respect to its long axis. The rotational diffusion of the molecule is larger at the ends than in the middle of the molecule. This finding may suggest that this mesogenic molecule undergoes rotational diffusion around its long axis with a type of motion that is similar to rotational diffusion in a cone model [20, 22].

The authors would like to thank the National Science Council of the Republic of China for financial support of this work under Contract No. NSC-84-2216-E007-029. This work was also financially supported by the National Centre for High-Performance Computing in Taiwan.



## References

[1] Gray, G. W., and Goodby, J. W., 1984, *Smectic Liquid Crystals: Textures and Structures* (Leonard-Hill).
[2] Blinov, L. M., and Chigrinov, V. G., 1994, *Electrooptic Effects in Liquid Crystal Materials* (Springer-Verlag).
[3] Bahadur, B., 1990, *Liquid Crystals: Applications and Uses* (World Scientific), Vol. 1.
[4] Hsu, C.-S., Shih, L.-J., and Hsiue, G.-H., 1993, *Macromolecules*, **26,** 3161.
[5] Chen, J.-H., Chang, R.-C., Hsiue, G.-H., Guu, F.-W., and Wu, S.-L., 1995, *Liq. Cryst.*, **18,** 291.
[6] Hsiue, G.-H., and Chen, J.-H., 1995, *Macromolecules*, **28,** 4366.
[7] Hsiue, G.-H., Wu, J.-L., and Chen, J.-H., 1996, *Liq. Cryst.*, **21,** 449.
[8] Lee, K.-J., Hsiue, G.-H., Wu, J.-L., and Chen, J.-H., 1998, *Liq. Crystals*, **25,** 661.
[9] Dodge, R., and Mattice, W. L., 1991, *Macromolecules*, **24,** 2709.
[10] Zhan, Y., and Mattice, W. L., 1992, *Macromolecules*, **25,** 1554.
[11] Zhan, Y., and Mattice, W. L., 1992, *Macromolecules*, **25,** 3439.
[12] Zhan, Y., and Mattice, W. L., 1992, *Macromolecules*, **25,** 4078.
[13] Zhan, Y., and Mattice, W. L., 1992, *J. chem. Phys.*, **96,** 3279.
[14] Lee, K.-J., Mattice, W. L., and Snyder, R. G., 1992, *J. chem. Phys.*, **96,** 9138.
[15] Vold, R. L., Vold, R. R., and Heaton, N. J., 1989, *Adv. Magn. Reso.*, **13,** 17.
[16] Souaille, M., Guillaume, F., and Smith, J. C., 1996, *J. chem. Phys.*, **105,** 1516.
[17] Souaille, M., Guillaume, F., and Smith, J. C., 1996, *J. chem. Phys.*, **105,** 1529.
[18] Jelinski, L. W., 1985, *Annu. Rev. mater. Sci.*, **15,** 359.
[19] Barbara, T. M., Vold, R. R., and Vold, R. L., 1983, *J. chem. Phys.*, **79,** 6338.
[20] Selwyn, L. S., Vold, R. L., and Vold, R. R., 1984, *J. chem. Phys.*, **80,** 5418.
[21] Barbara, T. M., Vold, R. R., Vold, R. L., and Neubert, M. E., 1985, *J. chem. Phys.*, **82,** 1612.
[22] Vold, R. R., and Vold, R. L., 1988, *J. chem. Phys.*, **88,** 1443.
[23] Goetz, J. M., Hoatson, G. L., and Vold, R. L., 1992, *J. chem. Phys.*, **97,** 1306.
[24] Greenfield, M. S., Vold, R. L., and Vold, R. R., 1985, *J. chem. Phys.*, **83,** 1440.
[25] Sekiya, T., Yuasa, K., Uchida, S., Hachiya, S., Hashimoto, K., and Kawasaki, K., 1993, *Liq. Cryst.*, **14,** 1255.
[26] Cannarozzi, G. M., Meresi, G. H., Vold, R. L., and Vold, R. R., 1991, *J. phys. Chem.*, **95,** 1525.
[27] Imashiro, F., Kuwahara, D., Nakai, T., and Terao, T., 1989, *J. chem. Phys.*, **90,** 3356.
[28] Sozzani, P., Bovey, F. A., and Schilling, F. C., 1991, *Macromolecules*, **24,** 6764.
[29] Doherty, D. C., and Hopfinger, A. J., 1991, *Computer Simulation of Polymers*, edited by R. J. Roe (Prentice-Hall), p. 55.
[30] Suehiro, J., and Takayanagi, M., 1970, *J. macromol. Sci., Phys.*, **B4,** 39.

[31] Wilson, M. R., and Allen, M. P., 1992, *Liq. Cryst*., **12,** 157.
[32] Wilson, M. R., and Allen, M. P., 1993, *Mol. Phys*., **80,** 277.
[33] Aoki, K. M., Yonezawa, F., 1993, *Liq. Cryst*., **14,** 1237.
[34] La Penna, G., Catalano, D., and Veracini, C. A., 1996, *J. chem. Phys*., **105,** 7097.
[35] Molecular Simulations Inc., 9685 Scranton Road, San Diego, CA, USA.
[36] Mayo, S. L., Olafson, B. D., and Goddard, W. A., 1990, *J. phys. Chem*., **94,** 8897.
[37] Rappé, A. K., and Goddard, W. A., 1991, *J. phys. Chem*., **95,** 3358.
[38] Cerius$^2$ Simulation Tools in User's Reference, Molecular Simulations Inc., 9685 Scranton Road, San Diego, CA, USA.
[39] Nosé, S., 1984, *J. chem. Phys*., **81,** 511.
[40] Nosé, S., 1984, *Mol. Phys*., **52,** 255.
[41] Allen, M. P., and Tildesley, D. J., 1987, *Computer Simulation of liquids* (Oxford: Clarendon Press).
[42] Ishaq, M., Blackwell, J., and Chvalun, S. N., 1996, *Polymer*, **37,** 1765.